CREaTor: Zero-shot *cis*-regulatory pattern modeling with attention mechanisms

Yongge Li[1,2,5], Fusong Ju[1,5], Zhiyuan Chen[1,3,5], Yiming Qu[1,4], Huanhuan Xia[1], Liang He[1], Lijun Wu[1], Jianwei Zhu[1], Bin Shao[1], Pan Deng[1,*]

[1]Microsoft Research AI4Science, Beijing, China. [2]School of Medicine, Tsinghua University, Beijing, China. [3]School of Computing, Australian National University, Canberra, Australia. [4]School of Life Sciences, Tsinghua University, Beijing, China. [5]These authors contributed equally: Yongge Li, Fusong Ju, and Zhiyuan Chen.

∗Correspondence: pan.deng@microsoft.com

Abstract

Linking *cis*-regulatory sequences to target genes has been a long-standing challenge. In this study, we introduce CREaTor, an attention-based deep neural network designed to model *cis*-regulatory patterns for genomic elements up to 2Mb from target genes. Coupled with a training strategy that predicts gene expression from flanking candidate *cis*-regulatory elements (cCREs), CREaTor can model cell type-specific *cis*-regulatory patterns in new cell types without prior knowledge of cCRE-gene interactions or additional training. The zero-shot modeling capability, combined with the use of RNA-seq and ChIP-seq data only, allows for the readily generalization of CREaTor to a broad range of cell types. Evaluation reveals that CREaTor outperforms existing methods in capturing cCRE-gene interactions across various distance ranges in held-out cell types. Further analysis indicates that the superior performance of CREaTor can be attributed to its capacity to model regulatory interactions at multiple levels, including the higher-order genome organizations that govern cCRE activities as well as cCRE-gene interactions. Collectively, our findings highlight CREaTor as a powerful tool for systematically investigating *cis*-regulatory programs across various cell types, both in normal developmental processes and disease-associated contexts.

Keywords:
gene regulation, *cis*-regulatory pattern, enhancer-gene interaction, gene expression, epigenetics

Background

Cell type-specific *cis*-regulatory programs allow specialized gene expression and cellular functions in eukaryotic organisms during development and differentiation (1–3). Mutations in *cis*-regulatory elements (CREs), though having no impact on protein sequences, contribute to various diseases by disrupting the normal functionality of their target genes (4–9). Decoding how CREs regulate gene expression coordinately in different cell types may reveal the mechanisms of cell identity maintenance and hint at the origins of developmental defects and human diseases.

However, linking candidate CREs (cCREs) to genes remains a substantial challenge. Experimental assays such as Hi-C (10), capture Hi-C (11), and ChIA-PET (12) have been deployed for cCRE-gene mapping, yet they measure physical proximities between elements and genes instead of direct regulatory activities. Systematic evaluation of activities of enhancers, a major type of CREs, becomes possible with CRISPR perturbation tools most recently (13–15), but only a subset of enhancers can be evaluated due to the great number of candidate enhancers in the genome (16,17). Meanwhile, the evaluations are restricted to the cell types examined in the studies.

Computational-based data-driven methods have been proposed for enhancer regulation prediction (18–22), but their performance and generalization ability are subject to limited data on *bona fide* enhancer-gene interactions, the varying number of candidate enhancers for different genes, and the complex nature of enhancer-gene regulation (7,23–25). Lack of native context during modeling is another drawback commonly seen due to a trade-off for computational feasibility. A typical case is the binary classification task where a sequence pair of enhancer and promoter is given as input (18–20), which may only recover regulation relationships mediated by conserved transcription factors universally present.

Interestingly, modeling studies on gene expression prediction from local genome sequences showed that cCRE-gene interactions were implied in the designed neural network architecture (26–28), suggesting an alternative approach for enhancer activity modeling. However, since different cell types in the same organism share the same reference genome, the sequence-based models such as Basenji2 (26) and Enformer (27), which take reference genome as input, cannot predict the activities of cell type-specific *cis*-regulatory sequences in cell types unseen by the model. While GraphReg (28) introduced a model architecture that can be generalized to new cell types, the model's dependency on 3D genomic data narrows its applicability, as such data is not readily available.

To model cCRE-gene interactions and discover universal *cis*-regulatory patterns across cell types, we developed a hierarchical deep learning model based on the self-attention mechanism. The model named CREaTor (*Cis*-Regulatory Element auto Translator) utilizes cCREs in open chromatin regions identified by Encyclopedia of DNA Elements (ENCODE) together with ChIP-seqs of transcription factors and histone modifications (16,29) to predict the expression level of target genes. In the design, attention blocks serve as key components for accurate expression prediction, which is achieved by learning relationships between input cCREs and genes, as well as cCREs and cCREs, during training. Therefore, leveraging attention mechanisms and training on richly labeled data generated through standardized experiments, we are able to model element interactions with a zero-shot setting. In other words, the model can present cCRE-gene interactions without requiring training on such data. Moreover, since CREaTor uses cCRE landscape and ChIP-seq profiles as input, which differ between cell types, it can model CRE-gene interactions in new cell types without additional training. Using dispersed elements instead of the entire genomic context flanking each gene also greatly reduces computational costs for modeling. Testing on a held-out cell line, we show that CREaTor can effectively model the interactions between *cis*-regulatory sequences and target genes for accurate gene expression prediction. Further analysis indicates that CREaTor learns higher-order genome organization and cross-cell type regulatory mechanisms, which might explain its exceptional performance in cell types unseen by the model.

Results

CREaTor predicts cell type-specific gene expression in unseen cell types. CREaTor consists of two transformer models at different resolutions (Fig. 1a and Extended Data Fig. 1). Transformer is a deep learning architecture that has been demonstrated as a powerful tool for natural language processing (30–32), computer vision (33,34), and biological modeling (27,35,36). A core component of a transformer is the self-attention module, which extracts sequence-level information by modeling the interactions between elements at different positions in the sequence (30). In CREaTor, the lower-level transformer (element encoder) learns the latent representation for each cCRE from the DNA sequence and chromatin states of the element itself, while the upper-level transformer (regulation encoder) predicts gene expression from a collection of cCRE latent representations flanking the target gene. Self-attention extracted from the regulation encoder is used to interpret the cCRE-gene and cCRE-cCRE interactions.

We trained CREaTor on 19 human tissues and cell lines whose annotated cCRE information was available in SCREEN Registry (16) (Supplementary Table 1). In each cell

type, chr16 was left out for validation, chr8 and 9 were left out for testing (*in-cell type test chromosomes*), and all other autosomes were used for training (Fig. 1b and Supplementary Figure 1). By training the model with data from multiple cell types jointly, we expected the model to learn general rules guiding gene regulation across cell types. Next, we evaluated CREaTor's performance on autosomes of the K562 cell line (*cross-cell type test chromosomes*), which were unseen by the model, to demonstrate the generalizability of our method (Fig.1b and Supplementary Figure 1). For the in-cell type test chromosomes, CREaTor reached a mean correlation of 0.850 and 0.818 (Pearson *r*) for chr8 and 9 respectively (Fig.1c and Extended Data Table 1). While for the cross-cell type test chromosomes, the correlations between observed and predicted gene expression on different chromosomes ranged from 0.756 to 0.936, with a mean correlation of 0.902 (Pearson *r*) (Fig. 1c and Extended Data Table 2). Notably, the predictive accuracy of K562 chr8 and 9 (0.839 and 0.810 respectively, Pearson *r*) was comparable to that of in-cell type test chromosomes, suggesting that CREaTor can predict gene expression efficiently from cCREs in new cell types.

However, the performance gap between chr8/9 and other chromosomes in K562 is non-trivial. We reasoned that the presence of housekeeping genes and several hematopoietic cell types in training data alleviated the challenge for expression prediction on chromosomes other than 8 and 9. To assess the generalizability of CREaTor more rigorously, we next examined if CREaTor could make cell type-specific predictions. With gene differential expression (GDE) analysis on paired data between K562 and each of the 19 cell types used for model training respectively, we identified 410 genes that were differentially expressed in the K562 cell line (Methods). For a number of these genes, including hematopoietic regulators KLF1 and TAL1 and hemoglobin subunit protein HBE1, CREaTor made a prediction on rival with experimental quantifications (Extended Data Fig. 2). In addition, single-linkage clustering analysis demonstrated that the prediction on K562 differentially expressed genes was more similar to observed K562 expression compared to other cell types (Pearson r≈0.68, Fig. 1d).

To further demonstrate that the accurate prediction of K562 expression is not attributed to the similarity between K562 and training cell types, we compared the predicted expressions with 122 observed expression profiles of 20 distinct cell types. These profiles included 12 profiles from 3 independent K562 RNA-seq experiments that our model had not previously encountered. We visualized all expression profiles with Uniform Manifold Approximation and Projection (UMAP) in a 2-dimensional space. For different chromosome subsets, predicted expression consistently exhibits high similarity to K562, as opposed to other cell types, including those sharing hematopoietic origins with K562 (Supplementary

Figure 2). Also, we conducted leave-one-chromosome-out and leave-one-cell type-out experiments to confirm that CREaTor's superior performance was not limited to chr8-9 and K562, respectively (Supplementary Figure 3 and Supplementary Table 2).

It has been reported that histone modifications and DNA openness proximal to gene transcription start sites (TSS) are significantly correlated with active transcription (37). To demonstrate that distal information contributes to model performance, we compared models trained with cCREs up to 2kb, 5kb, 10kb, 100kb, or 1Mb away from the TSS of target genes. Performance improved with increasing candidate window sizes (Extended Data Fig. 3), suggesting that CREaTor predicts gene expression from both proximal and distal cCREs. Also, this result indicates that distal cCREs are substantial for accurate expression prediction, supporting the importance of long-range *cis*-regulatory interactions in gene regulation. But meanwhile, it is worth noting that the model trained with cCREs up to 2kb away from target genes performed significantly better than random guesses, consistent with the knowledge that the proximal functional genomes and cCREs are closely related to gene expression.

Self-attention reveals functional cCREs in unseen cell types. Attention weights between cCREs and target genes extracted from CREaTor (Methods) may be exploited to interpret the importance of each cCRE to genes. To test this hypothesis, we benchmarked CREaTor against 3 CRISPR-based experimental-validated K562 enhancer-target gene datasets (13–15). To be noted, criteria for candidate enhancers vary in each study and few enhancer-target gene pairs tested were shared among studies (Extended Data Fig. 4 and Supplementary Table 3). Thus, we combined the experimental results and identified 1859 putative enhancers related to 328 genes that were tested by both the experimental approaches and CREaTor across the K562 genome. CREaTor prioritizes positive enhancer-gene pairs to negative ones with larger attention scores (auROC=0.834, auPRC=0.620; Fig. 2a-b) and the performance is further improved when we adjusted the attention scores with enhancer-gene genomic distances (auROC=0.843, auPRC=0.667; Fig. 2a-b). In addition, we compared the scores derived from the attention weights of CREaTor with a quantitative analysis of enhancer effects as described in a previous study (13). In this study, the enhancer effect on gene expression was defined as the change in gene expression upon enhancer knockdown using CRISPR perturbation. Consequently, the quantitative effect is inversely related to the enhancer activity. In line with this understanding, we observed a negative correlation, with a Spearman ρ of -0.269, between the CREaTor scores and the quantitative observations (Fig. 2c), implying that CREaTor captures quantitative effects of cCREs to genes.

We also compared CREaTor with 4 methods previously used for cCRE-gene interaction modeling: 1) Predictions based solely on genomic distances between cCREs and genes; 2) Predictions based on cCRE H3K27ac signals and cCRE-gene distances (approximate version of the Activity-by-Contact (ABC) score(13)). These model-free approaches can estimate activities of cCREs spanning varying ranges without prior knowledge of *cis*-regulatory programs in any cell types, or cell types with H3K27ac quantifications, which align well with the setting of CREaTor. Evaluated on a comprehensive set of metrics, CREaTor outperforms both methods at different distance groups (Fig. 2a-b and Extended Data Fig. 5). In addition, we compared CREaTor to 2 state-of-the-art deep learning approaches, 3) Enformer (27) and 4) GraphReg (28). Both Enformer and GraphReg, trained with supervised gene expression prediction tasks, support zero-shot cCRE-gene interaction prediction. However, Enformer's architecture limits it from long-range enhancer-gene interaction prediction, as the released Enformer model can only predict interactions up to 200kb. Additionally, it cannot generalize to new cell types as it solely relies on genomic sequences for predictions. To simulate prediction tasks in new cell types, we adopted the cell-type-agnostic setting of Enformer (Methods). As expected, predicting enhancer-gene interactions in new cell types with Enformer is not favorable (Fig. 2a-b and Extended Data Fig. 5). GraphReg, on the other hand, predicts CAGE signals from 1D epigenomic data and 3D genomic structures, allowing it to generalize to new cell types. However, its dependency on 3D genomic structures and CAGE profiles narrows its applicability. To evaluate GraphReg, we trained an enhanced GraphReg model using 9 cell types and 16 types of epigenomic profiles from scratch and derived feature importance to estimate enhancer activities in K562 as suggested by the original study (Methods). Our results show that CREaTor greatly outperforms GraphReg (Fig. 2a-b and Extended Data Fig. 5), suggesting the superiority of CREaTor's design.

Next, cCRE-gene interactions discovered by CREaTor were further benchmarked against a genome-wide Pol II-mediated ChIA-PET dataset (38). Compared with CRISPR perturbation studies, ChIA-PET covers a broader range of genes and regulators, thus capturing more comprehensive interactions between genes and regulators. We recovered 6, 132, 740 cCRE-gene pairs (both positive and negative) across the K562 genome from ChIA-PET. To benchmark CREaTor and its counterparts, for each gene, we calculated auROC and auPRC of the corresponding cCRE-gene pairs stratified by their relative genomic distances. Among all, CREaTor shows the highest median auROC and auPRC for gene collections at all distance groups and greatly outperforms Enformer and GraphReg (Fig 2d-e). Strikingly, CREaTor performs substantially better at groups spanning longer ranges.

Since ChIA-PET captures physical proximities between genomic regions, false positives exist when active CRE-gene pairs are recovered from ChIA-PET. To benchmark our method more comprehensively, we calculated the precision and specificity scores for different methods considering that these metrics are less impacted by false positives. Consistently, CREaTor outperforms other methods (Extended Data Fig. 6), indicating that CREaTor can capture cCRE-gene interactions efficiently from genomic features flanking target genes in unseen cell types.

Lastly, we examined if our model recovered regulators of the oncogenic gene MYC (chr8: 127,735,434-127,742,951). cCREs of MYC disperse along genomic sequences to as far as 2 Mb downstream MYC TSS and active MYC regulators in K562 were identified by previous studies with various approaches(39–41). Therefore, we examined if CREaTor could pinpoint these regulators accurately. The result indicates that CREaTor prioritizes positive MYC cCREs with larger attention scores and captures active cCREs missed by other predictive approaches (Fig. 2f). In addition, 2 groups of sharp peaks are observed 2Mb downstream MYC TSS (Fig. 2f), in concordance with the existence of 2 distal super-enhancer regions of MYC. Since MYC is in both in- and cross-cell type test sets, we believe that CREaTor has learned general rules guiding cCRE-gene interactions in different cell types, rendering it an efficient tool for cCRE activity modeling in unseen cell types.

CREaTor captures chromatin domain boundaries in unseen cell types. Three-dimensional (3D) chromatin folding allows physical interactions between distal cCRE and genes and the information can also guide gene regulation modeling (13,28,42). Without incorporating 3D chromatin folding information in our model, we were curious to see if CREaTor captured the topological structure of the genome, considering that CREaTor precisely recovers cCRE-gene interactions even of long ranges.

Attention matrices extracted from the model imply not only the interactions between cCREs and genes, but also relationships between cCRE-cCRE pairs. To examine if the attention matrix reflects contact frequency between elements, we aggregated the attention matrix at 10kb resolution for each gene in K562 and compared the results to a high-resolution Hi-C study (10). In addition to observing similar checkerboard patterns between the attention matrix and Hi-C (Fig. 3a), we systematically evaluated the consistency between the attention matrix and topologically associating domains (TADs) by analyzing insulation scores (Methods). We calculated insulation scores from the attention matrix over 12,584 K562 TAD boundaries defined in a recent study (43). The average score across the genome shows a clear insulation pattern on boundaries, similar to that calculated from the Hi-C experiment (Fig. 3b). Meanwhile, no significant decrease over GM12878-specific TAD

boundaries (43) is observed with insulation scores calculated from either K562 attention matrix or K562 Hi-C (Fig. 3b), demonstrating that CREaTor captures K562-specific TAD boundaries. Together, the results show that CREaTor can infer cell type-specific topological structures of genomes in cells unseen by the model.

We reason that CREaTor infers genome structures by learning the insulating behaviors of CTCF-bound elements. Consistently, we found that paired CTCF-bound insulators flanking the same TAD domain showed significantly larger attention scores compared to either unmatched insulator pairs spanning multiple TADs, or pairs involving non-insulator CTCF-bound elements (Fig. 3c). Thus, CREaTor may predict gene expression and capture cCRE-gene regulation efficiently by modeling topological patterns of the genome.

CREaTor implies directional regulation between cCREs. It is long proposed that enhancers form hierarchical relationships with each other, yet the relationship is challenging to be disentangled with biological experiments. For example, Carleton et al. developed an enhancer interference technique (Enhancer-i) to study the combinational effects of distal regulatory regions on genes (44). They showed the interdependence between CISH-1 and CISH-2, two estrogen receptor α-bound enhancers of the cytokine signaling suppressor gene *CISH*. However, the detailed mechanism between interactions of CISH-1 and CISH-2 could not be elucidated. Here, we examined attention scores between cCREs within CISH-1 and CISH-2 regions (denoted as Cr1 and Cr2 respectively) and found that the attention from Cr1 to Cr2 is significantly larger than the other way around (Fig.3f). To rule out potential distance bias, we examined attention score distribution of 5773 genes whose cCRE-gene distances were similar to Cr1-*CISH* and Cr2-*CISH* (denoted as SDaCr1 and SdaCr2). Remarkably, no directional preference between SDaCr2 and SDaCr2 was observed (Fig.3f). Therefore, our results indicate that there could be a directional relationship between CISH1 and CISH2, which is driven by hierarchical regulation of enhancers. We thus believe that with further development, CREaTor has the potential to become a powerful tool for understanding the causal relationships within enhancer networks.

cCRE representations learned by CREaTor suggest a new role of CTCF-bound elements. To investigate how CREaTor perceives cCREs and their roles during gene regulation, we clustered cCREs by the 256-dimensional cCRE representations extracted from CREaTor and examined features enriched in each group.

While different cCRE types are enriched in different clusters (Fig. 4a-b), cCRE representations learned by our model better capture functional variations of elements compared to the classification of ENCODE. For instance, while cCREs are aggregated into

6 clusters, both cluster 0 and cluster 1 are enriched with proximal enhancer-like elements, cCREs that show enhancer-like signatures falling within 200bp of an annotated transcript start site (TSS) (16). However, proximal enhancer-like elements in cluster 0 are enriched for RNA polymerase II (Pol II) signals (Extended Fig. 7), markers of active transcription events, compared to those in cluster 1. Since promoter-like elements are also enriched in cluster 0 and enhancers are believed to be able to contribute to promoter activities (45), we reason that CREaTor learns the discrepancies between enhancer-like elements of different roles and therefore associates a subgroup of proximal enhancer-like elements with promoters. Meanwhile, the fuzzy boundaries between clusters may indicate the adaptable functions of elements for gene regulation captured by our model.

CTCF-only cCREs, which lack both enhancer-like signatures and promoter-like signatures, are more isolated from other elements, consistent with their insulator and looping functions (Fig. 4a). However, CTCF-only cCREs are clustered into 2 separate groups, while a subgroup of CTCF-only cCREs is aggregated with distal enhancer-like elements in cluster 5 (Fig. 4b). Compared to other clusters, cluster 5 shows a significant enrichment of H3K36me3 peaks (Fig. 4c), a histone modification associated with diverse functions in conjugation with different types of epigenetic markers (42,46–50), indicating a higher chromatin activity of these elements. Consistent with the result, genes close to CTCF-only cCREs in cluster 5 (denoted as CTCF-H3K36me3 elements) show higher expression values compared to those close to low H3K36me3 CTCF-only elements (Fig. 4d), suggesting a more active role in gene transcription of CTCF-H3K36me3 elements.

Depletion of repressive histone modification H3K27me3 also supports the greater activity of CTCF-H3K36me3 elements (Fig. 4e). Other from H3K36me3, CTCF-H3K36me3 elements are enriched with H3K79me2 and H4K20me1 (Fig. 4e), a pattern that has been previously reported to be associated with active transcription and splicing of exons(46). Meanwhile, CTCF-H3K36me3 elements show increased H3K4me1 and H2AFZ signals (Fig. 4e), both of which are associated with enhanced transcription elongation(51,52). Considering a majority of CTCF-H3K36me3 elements locate outside exon regions, we propose that CTCF-H3K36me3 elements promote transcription elongation by serving as binding hubs for various *cis*- and *trans*-regulatory elements (Fig. 4f), which are captured by CREaTor for cross-cell type gene regulation modeling.

Discussion

While profiling gene expressions and epigenetic modifications in various cell types is feasible, systematical approaches profiling cell type-specific *cis*-regulatory patterns are currently not achievable. As a result, deep learning techniques, despite greatly advancing our understanding of gene regulation in many areas, face challenges in this area due to the lack of training data. To overcome this challenge, we introduce the CREaTor framework. By strategically selecting training tasks and incorporating attention mechanism, CREaTor enables zero-shot *cis*-regulatory pattern modeling and cCRE-gene interaction prediction

at ultra-long range. In addition, it can generalize to new cell types without requiring additional training or relying on 3D genomic data, making CREaTor versatile and applicable to a wide variety of cell types.

Comprehensive validation and benchmark experiments show that our model outperforms alternative methods in modeling cCRE-gene interactions. Additionally, attention analysis shows that CREaTor learns cell type-specific 3D genome interactions and insulation behaviors, which play crucial roles in gene regulation, during gene expression prediction. These results indicate that our model is able to capture the underlying principles that guide cCRE-gene interactions across different types of cells, utilizing 1D features such as histone modifications on the genome. Further experiments showcase that CREaTor captures regulatory mechanisms at multiple levels. Aside from cCREs, CREaTor also learns gene interpretations during modeling. Our model stratifies genes into distinct groups enriched with different biological processes and molecular functions (Extended Data Fig. 8), indicating that CREaTor has captured active pathways mediated by different transcription factor programs, which allow cell type-specific gene regulation by binding to cCREs. These analyses may explain how our model captures *cis*-regulatory patterns from a range of cross-cell type gene expression predictions.

Except for modeling cross-cell type *cis*-regulatory patterns, the adoption of transformer architecture has allowed for greater flexibility during application. For instance, the element module in CREaTor can handle candidate regulators of different lengths. Also, the regulation module allows the modeling of gene context with varying numbers of cCREs spanning varying genomic ranges. In addition, despite 17 types of input features being used for training, our model can still predict gene expression and infer cCRE-gene interactions when some features are missing, though a lack of features may negatively impact the performance of the model (Fig. 5a). Overall, this flexibility makes CREaTor more adaptable to different situations compared to other methods.

In order to assess the impact of each input feature on predicting gene expression and modeling *cis*-regulatory patterns, we conducted an ablation study by excluding individual feature types from the model's training. Our results revealed inconsistent performance between different tasks - while genome sequence information is dispensable for successful cell type-specific gene expression prediction, it has a moderate impact on the accuracy of CRE-gene interaction inference (Fig. 5b). Likely due to complementary relationships between different feature types, no single feature was found playing a dominant role in CRE-gene interactions. However, the exclusion of any feature type leads to decreased performance for CRE-gene interaction inference, and the model trained with a full collection of features performs significantly better on the cCRE-gene interaction classification task compared to all other settings (Fig. 5b), suggesting that utilization of multiple types of features guarantees our model's performance across cell types and CREaTor may have learned synergistic relationships between features for accurate *cis*-regulatory pattern modeling. Among all, features that are known to be crucial for gene regulation, such as CTCF, DNase, H3K4me3, H3K27ac, H3K9ac and EP300 show greater

384 importance. Pol II with enriched phosphorylated Ser5 in CTD is more important for gene
385 expression prediction and cCRE-gene interaction inference than its unphosphorylated form.
386 This could be explained by the active involvement of phosphorylated CTD in binding *trans*-
387 and *cis*-regulatory elements for dynamic transcription regulation. Evaluating the impact of
388 different Pol II phosphorylation states on gene regulation modeling in the future might give
389 additional insight into their roles. Interestingly, the results imply a paradoxical role of
390 H3K36me3 in gene regulation. This may be due to the fact that the gene sets regulated by
391 H3K36me3 are not included in the CRISPR perturbation experiments.
392
393 It is worth pointing out that our model's performance is constrained by the limited
394 accessibility of functional genomic data, regardless of the features employed. Although the
395 ENCODE project provides various high-quality functional genomic data of many cell types,
396 the coverage is still limited due to the vast number of cell types, histone modifications, and
397 proteins binding to the genome. For example, cohesin, which regulates chromatin structure
398 by participating in the loop extrusion process, was not included in our model data at the
399 time of modeling due to the lack of data in most cell types. We believe that incorporating
400 such data would further improve the generalizability of our method.
401
402 Compared to previous approaches, CREaTor is able to capture distal *cis*-regulatory
403 patterns and infer cCRE-gene interactions spanning ultra-long distances. We believe that
404 one reason for this improvement is the fact that our model was trained using only cCREs.
405 However, it is also important to note that this approach may lead to bias and neglect of
406 atypical regulators, such as non-canonical enhancers and other low-H3K27ac regulatory
407 elements without typical enhancer chromatin features (53,54). We expect that an end-to-
408 end setting incorporating a deep learning module calling CREs directly from the genome
409 will alleviate the issue of bias and allow for a more comprehensive understanding of *cis*-
410 regulatory elements.
411
412 Finally, in the interest of simplicity and consistency with previous studies, we have chosen
413 to utilize reference genomes during the training process. However, it is important to note
414 that functional genomic data on ENCODE might have originated from cells with different
415 genomes. Specifically, cell lines may exhibit different nucleotide polymorphisms, structural
416 variations, and karyotypes. As previous studies have demonstrated the predictive
417 capability of genomic sequences in various tasks (26,27,55,56) and we have shown that
418 the absence of sequences negatively impacts the performance of cCRE-gene interaction
419 inference (Fig. 5a), we anticipate that improved model performance will be garnered by
420 considering the diverse variations and associated consequences of different cell types in
421 future work. Despite these limitations, we believe that CREaTor can serve as a powerful
422 tool for studying cell type-specific *cis*-regulatory patterns and gene regulation networks,
423 with further improvements to be made in the future.
424
425

Methods

Model

Model architecture. The backbone of CREaTor is composed of two modules: (1) an element module to extract features of cCREs and (2) a regulation module to model the regulations between cCRE and genes.

CREaTor takes 200 cCREs from up- and down-stream of target gene TSS respectively as input (Note: we have also tried taking cCREs within the ± 1Mb range of a gene TSS for training. The outcomes of both strategies are comparable). Each element is represented by its DNA in the form of one-hot encoding (A = [1, 0, 0, 0, 0], T = [0, 1, 0, 0, 0], C = [0, 0, 1, 0, 0], G = [0, 0, 0, 1, 0], N = [0, 0, 0, 0, 1]) and ChIP-seq/DNase-seq with read-depth normalized signal or fold change over control, although the absence of ChIP-seqs can be tolerated by our proposed framework. We map the input DNA and ChIP-seq/DNase-seq to DNA embedding and ChIP-seq embedding through a linear projection to 256 channels respectively. Then, we organize the feature embedding at each base pair (Emb_{bp}) as the sum of DNA embedding and ChIP-seq embedding.

The core of the element module is an element encoder based on transformer encoder architecture. Each transformer encoder layer consists of a multi-head self-attention sub-layer and a position-wise fully connected feed-forward network sub-layer[30]. In the self-attention sub-layer, scaled dot-product attentions are performed as follows: embeddings calculate the query $Q \in \mathbb{R}^{n \times d_k}$, key $K \in \mathbb{R}^{n \times d_k}$, and value $V \in \mathbb{R}^{n \times d_v}$ through linear projection where n is the number of embeddings, d_k, d_v is the number of channels; the attention weight is calculated by $softmax(\frac{QK^T}{\sqrt{d_k}})$ representing the attention between pairwise; lastly, the value representing the semantics of all embeddings are aggregated according to the attention weights as shown in the equations below. Feed-forward network sub-layers introduce non-linearity and interact channel information. Since the transformer encoder is a position-agnostic architecture, we apply a relative positional embedding onto the attention weights to introduce positional information. We follow T5(57) to formulate the position embedding θ, where P is the relative position between base pairs within elements.

$$Attention(x) = softmax(\frac{(xW_q + b_q)(xW_k + b_k)^T}{\sqrt{d_k}} + \theta(P))(xW_v + b_v)$$

$$FFN(x) = max(xW_1 + b_1, 0)W_2 + b_2$$

We concatenate a learnable [CLS] token to Emb_{bp} in the element encoder. The [CLS] token adaptively attends Emb_{bp} and we use its output as the representation of elements (Emb_{ele}). The element encoder consists of 2 transformer encoder layers with 4 heads.

The regulation module comprises a regulation encoder to model the interactions between genes and cCREs and a prediction head for gene expression prediction.

Regulation encoder shares a similar architecture with element encoder, but with 4 transformer encoder layers and 4 attention heads. We concatenate [GENE] tokens and the corresponding cCRE embeddings Emb_{ele} to formulate the input of regulation encoder. To be noted, [GENE] tokens are initialized by shared learnable embeddings and different genes are distinguished by their associated TSS positions. Additionally, to ensure proper information flow, we mask out the attention weight between genes. Accordingly, [GENE] tokens adaptively attend Emb_{ele} and we use their output as the representation of genes (Emb_{gene}). Relative position P is calculated as the relative genomic distances of gene TSS and elements.

At last, we apply a prediction head comprised of a linear projection and a soft plus activation to predict the gene expression given gene representations Emb_{gene} output from the regulation encoder.

Model training. We trained our model with a batch size of 8 for 50, 000 steps using AdamW optimizer. For training stability, we warmed up the learning rate in the first 5, 000 steps from 0 to 1e-3 and linearly decayed it to 1e-8. Following previous work (26), we calculated the loss between the ground-truth and predicted values through a Poisson negative log-likelihood function. We also applied a gradient clip by norm with a maximum norm of 1.0 and a dropout rate of 0.1.

We verified the robustness of our model with 5 random seeds.

Attention score. Attention logit matrices were extracted from each attention layer in the Regulation Encoder. Both min-max and softmax normalization were applied based on needs. For cCRE-gene interaction modeling, we focused on attention from gene to cCRE only.

Training data

RNA expression, DNase-seq, and ChIP-seq files were downloaded from ENCODE (https://www.encodeproject.org/, by October 2021). For better quality control, we used experiments included in the reference human epigenomes (29) only (ENCODE-Reference epigenome matrix). The complete list of data can be found in Supplementary Table 4.

RNA-seq processing. Total RNA-seq and polyA plus RNA-seq data in human biosamples were downloaded from ENCODE. Released transcript quantifications mapped to the GRCh38 sequences and annotated to GENCODE V29 were retained. Gene expression level was calculated as the sum of transcript TPM. Log1p normalization was performed.

DNA-seq and ChIP-seq processing. DNase-seq, histone ChIP-seq, and TF ChIP-seq files of human biosamples mapped to the GRCh38 sequences were downloaded from ENCODE. Archived files were ignored. We kept read-depth normalized signal files for DNase-seq and fold change over control files for ChIP-seq.

cCREs. cCREs for different biosamples were downloaded from SCREEN Registry V3 (https://screen.encodeproject.org/, by October 2021). cCRE count for each biosample ranges from 85248 to 138179 (Supplementary Table 1). DNase-only and Low-DNase elements were removed. All elements were padded to 350bp for the convenience of modeling, which is not mandatory.

Cell types. We selected human tissues, primary cells, cell lines, and *in vitro* differentiated cells 1) with RNA-seq, DNase, CTCF ChIP-seq, H3K4me3 ChIP-seq, and H3K27ac ChIP-seq data available on ENCODE and 2) with complete cCRE information on SCREEN Registry V3.

CRE-gene interaction evaluation

Fulco et al. We downloaded the enhancer-gene interaction data from Supplementary Table 6a of the original study (13)**.** We converted genomic coordinates of candidate enhancers from hg19 to hg38 using the liftover program of the UCSC Genome Browser (https://genome.ucsc.edu/cgi-bin/hgLiftOver). Non-autosomal genes were removed.

Gasperini et al. We downloaded the data from Table S2 of the original study (14). We converted genomic coordinates of candidate enhancers from hg19 to hg38 using the liftover program of the UCSC Genome Browser. To generate gene-mapped negative samples from the Gasperini dataset, we first selected target genes from the identified 664 enhancer-gene pairs, and then picked out candidate enhancers within the 1Mb region of each target gene respectively from all enhancers screened. Non-autosomal genes were removed.

Schraivogel et al. We downloaded the data from Supplementary Table 2 and 3 of the original study (15). We converted genomic coordinates of candidate enhancers from hg19 to hg38 using the liftover program of the UCSC Genome Browser. To generate gene-mapped negative samples from the Schraivogel dataset, we first selected target genes from the identified 41 enhancer-gene pairs, and then picked out candidate enhancers within the 1Mb region of each target gene respectively from all enhancers screened.

ChIA-PET. We obtained the ChIA-PET data of K562 from the ENCODE portal (ENCSR880DSH). To evaluate the model's performance, for each gene, we used a total of 400 regulators upstream and downstream as the evaluation dataset. To calculate the cCRE-gene or cCRE-CRE interaction, for each pair of interacting sequences, we calculated whether the reads pair intersected the gene and CRE, respectively. The gene was considered to interact with the cCRE and regarded as a positive sample if crossed and as a negative sample otherwise.

ABC score. ABC score was adapted from Fulco et al(13). To be more specific, we collected the bigWig files of H3K27ac and DNase from ENCODE's ENCFF977KGH and ENCFF414OGC, respectively, and converted them to bedGraph files with the UCSC tool `bigWigTobedGraph`. For each cCRE, we determined its signal by calculating the sum of the signals intersecting with it. Accordingly, we calculated the ABC score as the geometric mean of the H3K27ac and DNase signals multiplied by the reciprocal of the distance between the cCRE and the TSS (27).

Classification of cCRE-gene interaction by distance groups. For each gene, the cCREs are divided into 4 groups (0-5kb, 5-50kb, 50-1000kb, 100-1000kb, 1000kb+) according to their distances to gene TSS. Groups with less than 10 gene-CREs pairs were filtered. auPRC and auROC for each group of each gene were calculated. For specificity and precision, we used mean values as the cutoff for the classification of positive and negative regulators.

Enformer(27)**.** Pre-trained Enformer model was downloaded from https://github.com/deepmind/deepmind-research/tree/master/enformer. Genomic sequences flanking genes of interest were prepared following the original study's instructions. Gradient x input of candidate enhancers was calculated following the original study's instructions. To be pointed out, to simulate prediction tasks in new cell types, we used the cell-type-agnostic setting during the analysis. More specifically, the gradient was calculated and aggregated from all human tracks of the model.

GraphReg(28)**.** Epi-GraphReg model was downloaded from https://github.com/karbalayghareh/GraphReg. Genomic sequences and DNase-seq, H3K27ac, H3K4me3 were prepared following the original study's instructions. For a fair comparison, we incorporated histone modifications and transcription factor (TF) binding profiles used for CREaTor training as well (see Supplementary Table 4 for a full list). For training, we sourced chromosomes from cell lines including GM12878, B cells, HeLa-S3, MCF-7, fibroblast of dermis, CD14 positive monocyte, H1, HepG2, and keratinocyte

(Supplementary Table 4c), deliberately excluding chromosomes Chr8, Chr9, and Chr16. The CAGE data for these cell lines were downloaded from ENCODE, as detailed in Supplementary Table 4c. We replaced the 3D genomic data with the reciprocal of the genomic distances between the cCRE and the TSS. For cCRE-gene interaction classification, we calculated saliency and integrated gradients for candidate enhancers following the original study's instructions. The feature attribution type led to the best performance was used for comparison.

TAD prediction

Hi-C data processing. We obtained the long-range chromatin interactions of K562Hi-C data from ENCODE (ENCSR545YBD). To estimate the interaction matrix with each cCRE as a bin, the Hi-C pairs that intersected with each cCRE pair were added together.

Calculation of insulation score. We calculated the sum of the interactions in each bin within 10kb as the Hi-C interaction matrix for 10kb resolution. A similar operation was applied to the attention matrix. We summed the min-max-normalized attention matrix within 10kb windows as the attention matrix at 10kb resolution. We obtained the location of the TAD boundary on K562 and GM12878 from the previous study (43). The interactions of the 3*3 matrix were summarized at one bin from the diagonal (58) to represent the insulation score for each TAD boundary. GM12878-specific TAD boundaries are genomics regions called in GM12878 boundary file exclusively.

Grouping of CTCF-bound elements. For all cCREs showing positive CTCF binding patterns, we determined whether they intersected with the TAD boundary from a previous study (43). We considered the intersecting cCREs as anchors of the TAD boundaries, and others as non-anchors. We extracted the attention scores between these CTCF-bound cCREs and then divided the weights into various groups. Scores for anchor cCRE pairs on the same TAD boundary were classified as "anchor-to-anchor"; scores between anchor cCRE and non-anchor cCRE within the same TAD were classified as "anchor-to-non-anchor"; scores for anchor cCREs on adjacent TADs were classified as "anchor-to-anchor in adjacent TADs"; and scores for anchor cCREs more than one TAD apart were classified as "anchor-to-anchor in remote TADs".

Mapping of CISH enhancers. First, we obtained the two regulatory loci Cp1 and Cp2 of CISH from the previous study(44) and converted their genomic coordinates from mm9 to mm10 using the `liftover` program of the UCSC Genome Browser. Then, for all cCREs of CISH genes in K562, we determined which cCREs intersected with Cp1 and Cp2, representing Cp1 and Cp2 respectively. Finally, we calculated the attention scores from

Cp1 to Cp2 in K562 cell line to determine the effect of Cp1 on Cp2; and from Cp2 to Cp1 to determine the effect of Cp2 on Cp1. The control background (SDaCp1 and SDaCp2) consisted of interactions between cCREs with the same distance from Cp1 and Cp2 to CISH to all protein-coding genes except CISH.

K562-specific genes. We obtained the expression data of each cell line's gene from ENCODE (Supplementary Table 4a). Using the expression data of K562 as a control, we extracted the count matrix of each other cell line by the function `rsem-generate-data-matrix` of RSEM. These count matrices were then used to calculate differentially expressed genes using the function `rsem-run-ebseq`. After that, we screened the genes with PPDE (posterior probability that a gene/transcript is differentially expressed) greater than 95% as differentially expressed genes for K562 versus each cell line. Finally, the intersection of these differential genes was considered K562-specific genes.

Representation clustering and visualization. First, we reduced the dimensionality of the 256-dimensional representations learned by our model with `scanpy.tl.pca` (default parameters). After a neighborhold graph is calculated (`scanpy.pp.neighbors`, `n_neighbors=20`, `n_pcs=50`), we clustered reduced representations with Leiden graph-clustering method (`scanpy.tl.leiden`, `resolution=0.5`). The neighborhood graph and clusters were then visualized using Uniform Manifold Approximation and Projection (UMAP).

Data Availability

RNA expression, DNase-seq, ChIP-seq, Hi-C, CAGE and ChIA-PET files were downloaded from https://www.encodeproject.org/ (Supplementary Table 4). cCREs for different biosamples were downloaded from SCREEN Registry V3 (https://screen.encodeproject.org/). Both K562 TAD boundary and GM12878 TAD boundary file were downloaded from https://drive.google.com/drive/folders/15Rc6PhrrBjThwE-5dSyNX-ILELaUu6uG. CRISPR perturbation experiments of enhancer-gene interactions were downloaded from reference 13-15 respectively.

Code Availability

The code for data processing, model training and evaluation are available at https://github.com/DLS5-Omics/CREaTor.

Acknowledgements

We thank Dr. Chuan Cao, Dr. Haiguang Liu, Dr. Bofeng Liu, Dr. Han Yuan, and Dr. Yanxiao Zhang for constructive suggestions and feedback; Dr. Tie-Yan Liu for project supervision; Shizhuo Zhang and Yifan Deng for discussions on modeling.

Authors' contributions

Conceptualization, P.D., Y.L., H.X. and Y.Q.; methodology and modeling, F.J., Z.C., P.D., H.X. and Y.Q.; data curation, P.D., Y.L., F.J. and Z.C.; result interpretation, P.D., Y.L., F.J., and Y.Q.; writing-original draft, P.D., Y.L., Z.C., Y.Q, and F.J.; writing-review, P.D., Y.L., Y.Q, H.X., Z.C., L.H., L.W., F.J., B.S. and J.Z.; supervision, B.S.. All authors read and approved the final manuscript.

Competing interests

The authors declare no competing interests.

Reference

1. Furlong EEM, Levine M. Developmental enhancers and chromosome topology. Science. 2018 Sep 28;361(6409):1341–5.

2. Long HK, Prescott SL, Wysocka J. Ever-changing landscapes: transcriptional enhancers in development and evolution. Cell. 2016 Nov 17;167(5):1170–87.

3. Plank JL, Dean A. Enhancer Function: Mechanistic and Genome-Wide Insights Come Together. Mol Cell. 2014 Jul 3;55(1):5–14.

4. Sakabe NJ, Savic D, Nobrega MA. Transcriptional enhancers in development and disease. Genome Biol. 2012 Jan 23;13(1):238.

5. Claringbould A, Zaugg JB. Enhancers in disease: molecular basis and emerging treatment strategies. Trends Mol Med. 2021 Nov 1;27(11):1060–73.

6. Sur I, Taipale J. The role of enhancers in cancer. Nat Rev Cancer. 2016 Aug;16(8):483–93.

7. Mumbach MR, Satpathy AT, Boyle EA, Dai C, Gowen BG, Cho SW, et al. Enhancer connectome in primary human cells identifies target genes of disease-associated DNA elements. Nat Genet. 2017 Nov;49(11):1602–12.

8. Nasser J, Bergman DT, Fulco CP, Guckelberger P, Doughty BR, Patwardhan TA, et al. Genome-wide enhancer maps link risk variants to disease genes. Nature. 2021 May;593(7858):238–43.

9. Smith E, Shilatifard A. Enhancer biology and enhanceropathies. Nat Struct Mol Biol. 2014 Mar;21(3):210–9.

10. Rao SSP, Huntley MH, Durand NC, Stamenova EK, Bochkov ID, Robinson JT, et al. A 3D Map of the Human Genome at Kilobase Resolution Reveals Principles of Chromatin

694 Looping. Cell. 2014 Dec;159(7):1665–80.

695 11. Mifsud B, Tavares-Cadete F, Young AN, Sugar R, Schoenfelder S, Ferreira L, et al. Mapping
696 long-range promoter contacts in human cells with high-resolution capture Hi-C. Nat
697 Genet. 2015 Jun;47(6):598–606.

698 12. Tang Z, Luo OJ, Li X, Zheng M, Zhu JJ, Szalaj P, et al. CTCF-Mediated Human 3D Genome
699 Architecture Reveals Chromatin Topology for Transcription. Cell. 2015 Dec
700 17;163(7):1611–27.

701 13. Fulco CP, Nasser J, Jones TR, Munson G, Bergman DT, Subramanian V, et al. Activity-by-
702 contact model of enhancer–promoter regulation from thousands of CRISPR
703 perturbations. Nat Genet. 2019 Dec;51(12):1664–9.

704 14. Gasperini M, Hill AJ, McFaline-Figueroa JL, Martin B, Kim S, Zhang MD, et al. A Genome-
705 wide Framework for Mapping Gene Regulation via Cellular Genetic Screens. Cell. 2019
706 Jan;176(1–2):377-390.e19.

707 15. Schraivogel D, Gschwind AR, Milbank JH, Leonce DR, Jakob P, Mathur L, et al. Targeted
708 Perturb-seq enables genome-scale genetic screens in single cells. Nat Methods. 2020
709 Jun;17(6):629–35.

710 16. The ENCODE Project Consortium, Moore JE, Purcaro MJ, Pratt HE, Epstein CB, Shoresh N,
711 et al. Expanded encyclopaedias of DNA elements in the human and mouse genomes.
712 Nature. 2020 Jul 30;583(7818):699–710.

713 17. Shen Y, Yue F, McCleary DF, Ye Z, Edsall L, Kuan S, et al. A map of the cis-regulatory
714 sequences in the mouse genome. Nature. 2012 Aug;488(7409):116–20.

715 18. Li W, Wong WH, Jiang R. DeepTACT: predicting 3D chromatin contacts via bootstrapping
716 deep learning. Nucleic Acids Res. 2019 Jun 4;47(10):e60–e60.

717 19. Hait TA, Amar D, Shamir R, Elkon R. FOCS: a novel method for analyzing enhancer and
718 gene activity patterns infers an extensive enhancer–promoter map. Genome Biol. 2018
719 Dec;19(1):56.

720 20. Whalen S, Truty RM, Pollard KS. Enhancer-promoter interactions are encoded by complex
721 genomic signatures on looping chromatin. Nat Genet. 2016 May;48(5):488–96.

722 21. Hariprakash JM, Ferrari F. Computational Biology Solutions to Identify Enhancers-target
723 Gene Pairs. Comput Struct Biotechnol J. 2019;17:821–31.

724 22. Cao Q, Anyansi C, Hu X, Xu L, Xiong L, Tang W, et al. Reconstruction of enhancer–target
725 networks in 935 samples of human primary cells, tissues and cell lines. Nat Genet. 2017
726 Oct 1;49(10):1428–36.

727 23. Schoenfelder S, Fraser P. Long-range enhancer–promoter contacts in gene expression

control. Nat Rev Genet. 2019 Aug;20(8):437–55.

24. Moore JE, Pratt HE, Purcaro MJ, Weng Z. A curated benchmark of enhancer-gene interactions for evaluating enhancer-target gene prediction methods. Genome Biol. 2020 Dec;21(1):17.

25. Oudelaar AM, Higgs DR. The relationship between genome structure and function. Nat Rev Genet. 2021 Mar;22(3):154–68.

26. Kelley DR. Cross-species regulatory sequence activity prediction. PLOS Comput Biol. 2020 Jul 20;16(7):e1008050.

27. Avsec Ž, Agarwal V, Visentin D, Ledsam JR, Grabska-Barwinska A, Taylor KR, et al. Effective gene expression prediction from sequence by integrating long-range interactions. Nat Methods. 2021 Oct;18(10):1196–203.

28. Karbalayghareh A, Sahin M, Leslie CS. Chromatin interaction aware gene regulatory modeling with graph attention networks [Internet]. bioRxiv; 2021 [cited 2022 Apr 18]. p. 2021.03.31.437978. Available from: https://www.biorxiv.org/content/10.1101/2021.03.31.437978v1

29. Roadmap Epigenomics Consortium, Kundaje A, Meuleman W, Ernst J, Bilenky M, Yen A, et al. Integrative analysis of 111 reference human epigenomes. Nature. 2015 Feb 19;518(7539):317–30.

30. Vaswani A, Shazeer N, Parmar N, Uszkoreit J, Jones L, Gomez AN, et al. Attention Is All You Need [Internet]. arXiv; 2017 Dec [cited 2022 May 16]. Report No.: arXiv:1706.03762. Available from: http://arxiv.org/abs/1706.03762

31. Devlin J, Chang MW, Lee K, Toutanova K. BERT: Pre-training of Deep Bidirectional Transformers for Language Understanding. ArXiv181004805 Cs [Internet]. 2019 May 24 [cited 2022 Apr 19]; Available from: http://arxiv.org/abs/1810.04805

32. [1907.11692] RoBERTa: A Robustly Optimized BERT Pretraining Approach [Internet]. [cited 2022 May 16]. Available from: https://arxiv.org/abs/1907.11692

33. Liu Z, Hu H, Lin Y, Yao Z, Xie Z, Wei Y, et al. Swin Transformer V2: Scaling Up Capacity and Resolution [Internet]. arXiv; 2022 [cited 2022 Oct 20]. Available from: http://arxiv.org/abs/2111.09883

34. Wang W, Bao H, Dong L, Bjorck J, Peng Z, Liu Q, et al. Image as a Foreign Language: BEiT Pretraining for All Vision and Vision-Language Tasks [Internet]. arXiv; 2022 [cited 2022 Oct 20]. Available from: http://arxiv.org/abs/2208.10442

35. Vaishnav ED, de Boer CG, Molinet J, Yassour M, Fan L, Adiconis X, et al. The evolution, evolvability and engineering of gene regulatory DNA. Nature [Internet]. 2022 Mar 9 [cited 2022 Mar 11]; Available from: https://www.nature.com/articles/s41586-022-04506-6

763 36. Jumper J, Evans R, Pritzel A, Green T, Figurnov M, Ronneberger O, et al. Highly accurate
764 protein structure prediction with AlphaFold. Nature. 2021 Aug 26;596(7873):583–9.

765 37. Wang Z, Chivu AG, Choate LA, Rice EJ, Miller DC, Chu T, et al. Prediction of histone post-
766 translational modification patterns based on nascent transcription data. Nat Genet. 2022
767 Mar;54(3):295–305.

768 38. ENCODE Project Consortium. An integrated encyclopedia of DNA elements in the human
769 genome. Nature. 2012 Sep 6;489(7414):57–74.

770 39. Schuijers J, Manteiga JC, Weintraub AS, Day DS, Zamudio AV, Hnisz D, et al.
771 Transcriptional Dysregulation of MYC Reveals Common Enhancer-Docking Mechanism.
772 Cell Rep. 2018 Apr 10;23(2):349–60.

773 40. Fulco CP, Munschauer M, Anyoha R, Munson G, Grossman SR, Perez EM, et al. Systematic
774 mapping of functional enhancer–promoter connections with CRISPR interference.
775 Science. 2016 Nov 11;354(6313):769–73.

776 41. Hnisz D, Abraham BJ, Lee TI, Lau A, Saint-André V, Sigova AA, et al. Super-Enhancers in
777 the Control of Cell Identity and Disease. Cell. 2013 Nov 7;155(4):934–47.

778 42. Lee D. Learning the histone codes with large genomic windows and three-dimensional
779 chromatin interactions using transformer. Nat Commun. 2022;19.

780 43. Stilianoudakis SC, Marshall MA, Dozmorov MG. preciseTAD: a transfer learning
781 framework for 3D domain boundary prediction at base-pair resolution. Robinson P,
782 editor. Bioinformatics. 2022 Jan 12;38(3):621–30.

783 44. Carleton JB, Berrett KC, Gertz J. Multiplex Enhancer Interference Reveals Collaborative
784 Control of Gene Regulation by Estrogen Receptor α-Bound Enhancers. Cell Syst. 2017
785 Oct 25;5(4):333-344.e5.

786 45. van Arensbergen J, FitzPatrick VD, de Haas M, Pagie L, Sluimer J, Bussemaker HJ, et al.
787 Genome-wide mapping of autonomous promoter activity in human cells. Nat Biotechnol.
788 2017 Feb;35(2):145–53.

789 46. Schwartz S, Meshorer E, Ast G. Chromatin organization marks exon-intron structure. Nat
790 Struct Mol Biol. 2009 Sep;16(9):990–5.

791 47. DiFiore JV, Ptacek TS, Wang Y, Li B, Simon JM, Strahl BD. Unique and Shared Roles for
792 Histone H3K36 Methylation States in Transcription Regulation Functions. Cell Rep. 2020
793 Jun;31(10):107751.

794 48. Joshi AA, Struhl K. Eaf3 Chromodomain Interaction with Methylated H3-K36 Links Histone
795 Deacetylation to Pol II Elongation. Mol Cell. 2005 Dec 22;20(6):971–8.

796 49. Carrozza MJ, Li B, Florens L, Suganuma T, Swanson SK, Lee KK, et al. Histone H3

797 Methylation by Set2 Directs Deacetylation of Coding Regions by Rpd3S to Suppress
798 Spurious Intragenic Transcription. Cell. 2005 Nov 18;123(4):581–92.

799 50. Bartke T, Vermeulen M, Xhemalce B, Robson SC, Mann M, Kouzarides T. Nucleosome-
800 Interacting Proteins Regulated by DNA and Histone Methylation. Cell. 2010 Oct
801 29;143(3):470–84.

802 51. Weber CM, Ramachandran S, Henikoff S. Nucleosomes Are Context-Specific, H2A.Z-
803 Modulated Barriers to RNA Polymerase. Mol Cell. 2014 Mar 6;53(5):819–30.

804 52. Henriques T, Scruggs BS, Inouye MO, Muse GW, Williams LH, Burkholder AB, et al.
805 Widespread transcriptional pausing and elongation control at enhancers. Genes Dev.
806 2018 Jan 1;32(1):26–41.

807 53. Pradeepa MM, Grimes GR, Kumar Y, Olley G, Taylor GCA, Schneider R, et al. Histone H3
808 globular domain acetylation identifies a new class of enhancers. Nat Genet. 2016
809 Jun;48(6):681–6.

810 54. Rajagopal N, Srinivasan S, Kooshesh K, Guo Y, Edwards MD, Banerjee B, et al. High-
811 throughput mapping of regulatory DNA. Nat Biotechnol. 2016 Feb;34(2):167–74.

812 55. Nair S, Kim DS, Perricone J, Kundaje A. Integrating regulatory DNA sequence and gene
813 expression to predict genome-wide chromatin accessibility across cellular contexts.
814 Bioinformatics. 2019 Jul 15;35(14):i108–16.

815 56. maxATAC: Genome-scale transcription-factor binding prediction from ATAC-seq with
816 deep neural networks | PLOS Computational Biology [Internet]. [cited 2023 Aug 24].
817 Available from:
818 https://journals.plos.org/ploscompbiol/article?id=10.1371/journal.pcbi.1010863

819 57. Raffel C, Shazeer N, Roberts A, Lee K, Narang S, Matena M, et al. Exploring the Limits of
820 Transfer Learning with a Unified Text-to-Text Transformer [Internet]. arXiv; 2020 [cited
821 2022 Oct 27]. Available from: http://arxiv.org/abs/1910.10683

822 58. Crane E, Bian Q, McCord RP, Lajoie BR, Wheeler BS, Ralston EJ, et al. Condensin-driven
823 remodelling of X chromosome topology during dosage compensation. Nature. 2015
824 Jul;523(7559):240–4.

825

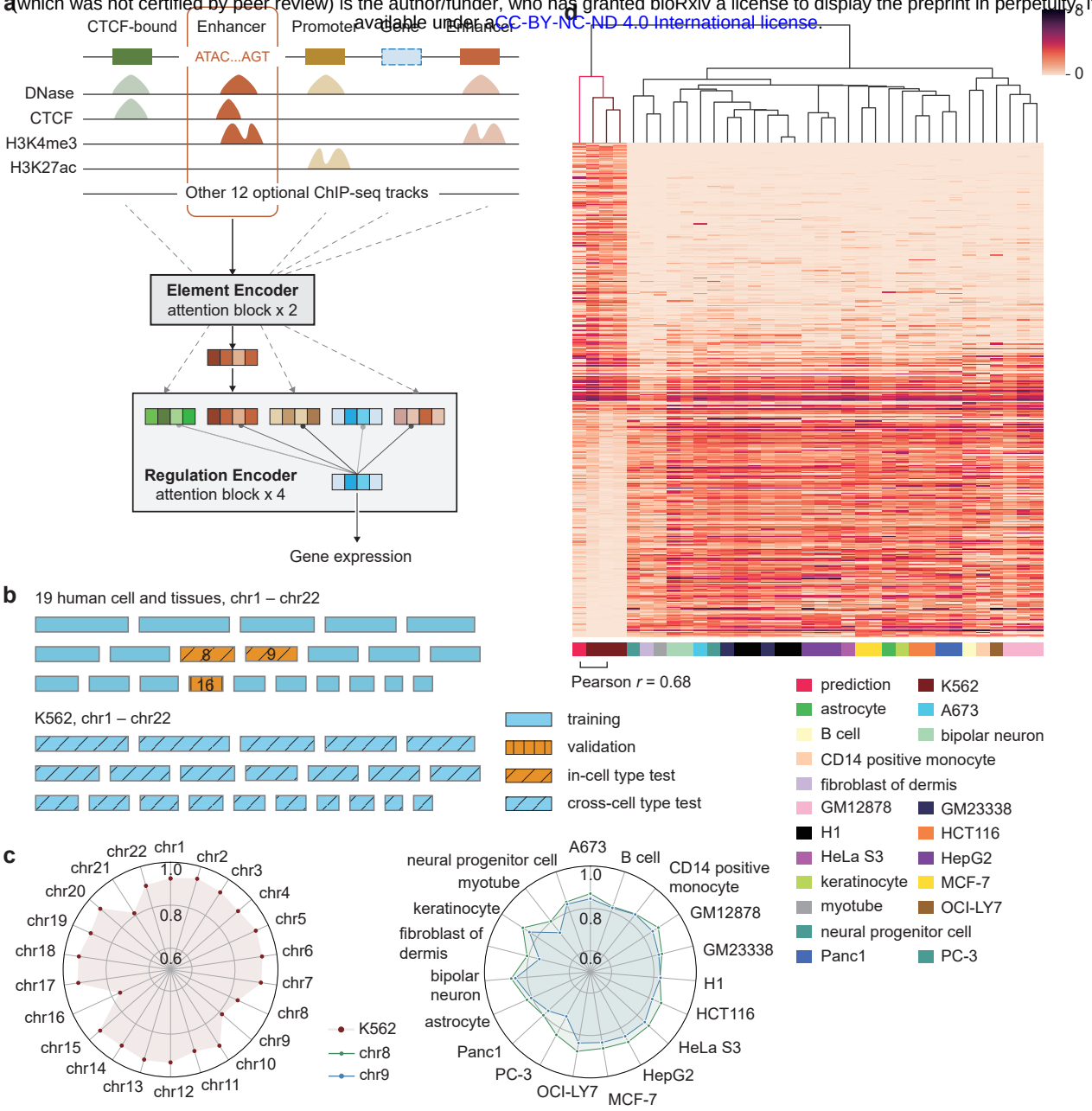

Figure 1. Accurate gene expression prediction with CREaTor. a) Schema of CREaTor. The model predicts target gene expression from the flanking cCREs with a hierarchical transformer structure. Localization of cCREs was obtained from ENCODE consortium. A combination of genomic sequences, chromatin openness, and a collection (3-13) of ChIP-seq profiles was used as input features for each cCRE. **b)** Visualization of data split strategy: we trained our model on gene expression of 19 autosomes from 19 different cell lines and tissues respectively. Genes on chr16 from the 19 cell lines and tissues were used for parameter tuning (validation), while genes on chr8, 9 were used for model evaluation (in-cell type test chromosomes). Genes from all autosomes in K562 (cross-cell type test chromosomes) were detailedly evaluated to demonstrate the model's ability on cross-cell type gene expression and regulation modeling. Also see in Supplementary Figure 1. **c)** Pearson *r* between observed and predicted expression of genes. Left: Pearson *r* between observed and predicted expressions of genes on cross-cell type test chromosomes. Right: Pearson *r* between observed and predicted expressions of genes on in-cell type test chromosomes. Green and blue dots indicate chr8 and 9 respectively. See Extended Data Table 2 for results with different random seeds. **d)** Clustering map of predicted and observed expression of K562 specific genes (calculated with RSME, see Methods) in different cell types. The leftmost column is the predicted value, which is clustered with the K562 observed gene expression data using the hierarchical clustering method. Expression values were transformed with log1p. Observed gene expression profiles from different sources (with different experiment IDs on ENCODE) for the same cell type are calculated independently.

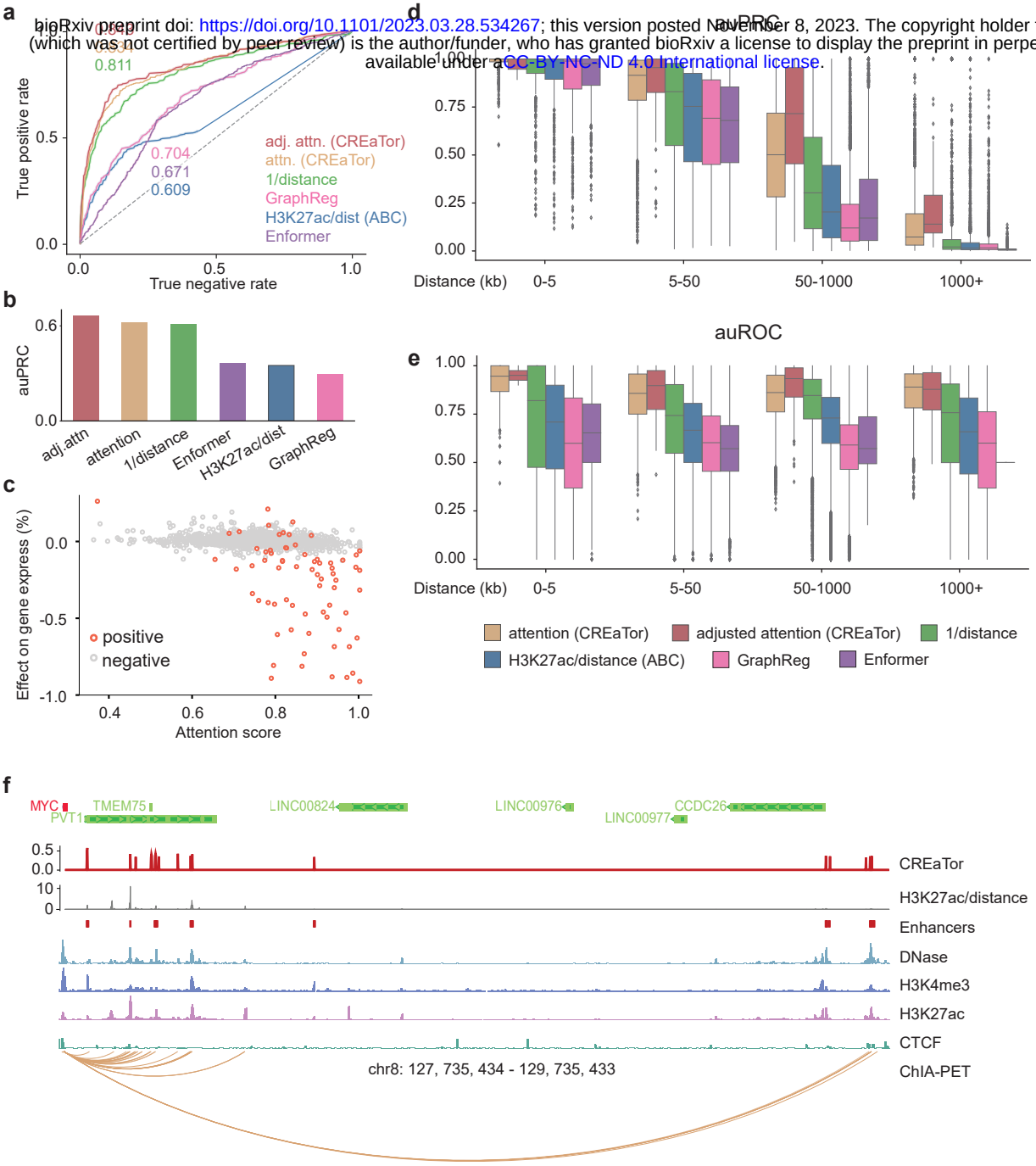

Figure 2. Attention matrix of CREaTor implies cCRE-gene interactions. a-b) auROC (a) and auPRC (b) of CREaTor outperform its counterparts on cCRE-gene pair classification. Attention (attn., yellow): normalized attention weights (genes to cCREs) in CREaTor. Adjusted attention (adj. attn., red): attention scores / log10 (distance). H3K27ac/dist (blue): approximate of the ABC score. Distance quantifies relative genomic distances between genes and cCREs. H3K27ac value of a cCRE is calculated as the sum of H3K27ac peak values of the element. Labels (positive/negative) of cCRE-gene pairs were collected from 3 independent CRISPR perturbation experiments. **c)** Attention scores derived from attention weights are significantly correlated with the effect of enhancer on gene expression quantified by Fulco et al[13]. As the quantification measures the change of target gene expression upon enhancer knock-down using CRISPR perturbation, the quantitative effect values are invertsely related to enhancer activities. **d-e)** auPRC (d) and auROC (e) of CREaTor and its counterparts on the classification of cCRE-gene pairs collected from a Pol-II mediated ChIA-PET experiment. The performance is evaluated for each gene and each distance group separately. Groups with <10 samples were filtered out. Center line, median; box limits, upper and lower quartiles; whiskers, 1.5x interquartile range; points, outliers. **f)** MYC locus showing predicted and previously reported regulators in K562 cells. For CREaTor (red) and H3K27ac/distance (gray), peaks on the tracks represent the scores of different cCRE regions. Enhancers track (red squares) denotes reported active regulators of MYC. Representative DNase, H3K4me3, H3K27ac and CTCF tracks as well as ChIA-PET interactions in K562, are also annotated.

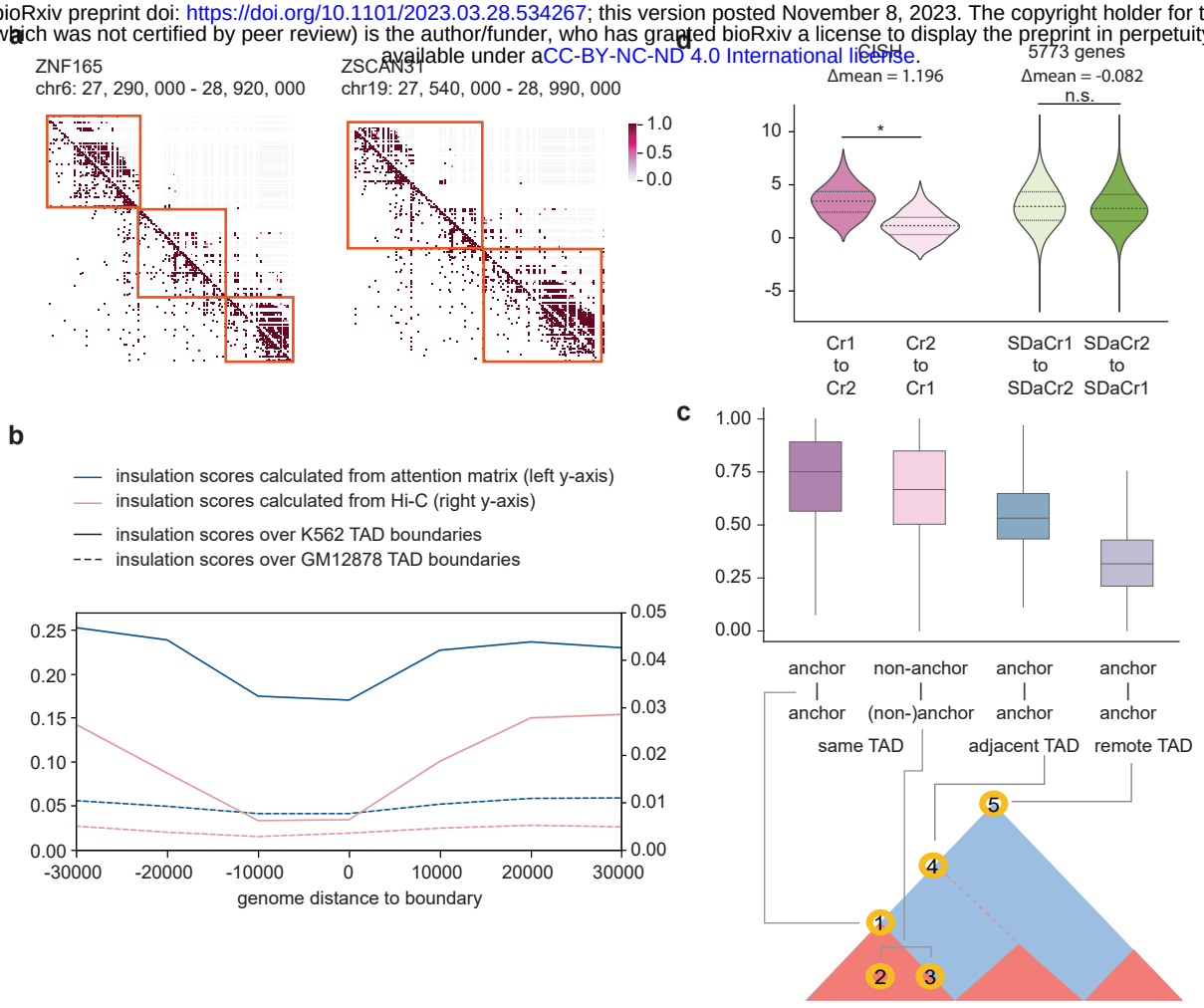

Figure 3. CREaTor captures hierarchically higher-order genome organizations. a) Example genomic regions showing the similarity between attention matrix (above the diagnal) and Hi-C contact matrix (below the diagonal). Orange boxes indicate TAD domains. **b)** Average insulation scores across the K562 genome at 10-kb resolution calculated from attention matrix and Hi-C. Blue line and left y-axis: insulation scores of attention matrix. Pink line and right y-axis: the insulation scores of Hi-C. Solid lines indicate insulation scores over K562 TAD boundaries and dashed lines indicate insulation scores over GM12878 boundaries. The x-axis is centered on TAD boundaries. **c)** Upper panel: Statistics of attention weights between CTCF-bound element pairs with different topological relationships. Center line, median; box limits, upper and lower quartiles; whiskers, 1.5x interquartile range. Lower panel: illustration of CTCF-bound element pairs used for the analysis. The red triangle represents TAD domains called from the Hi-C matrix (blue). **d)** Average attention scores between elements without normalization. p-value is calculated with Mann-Whitney U Test.

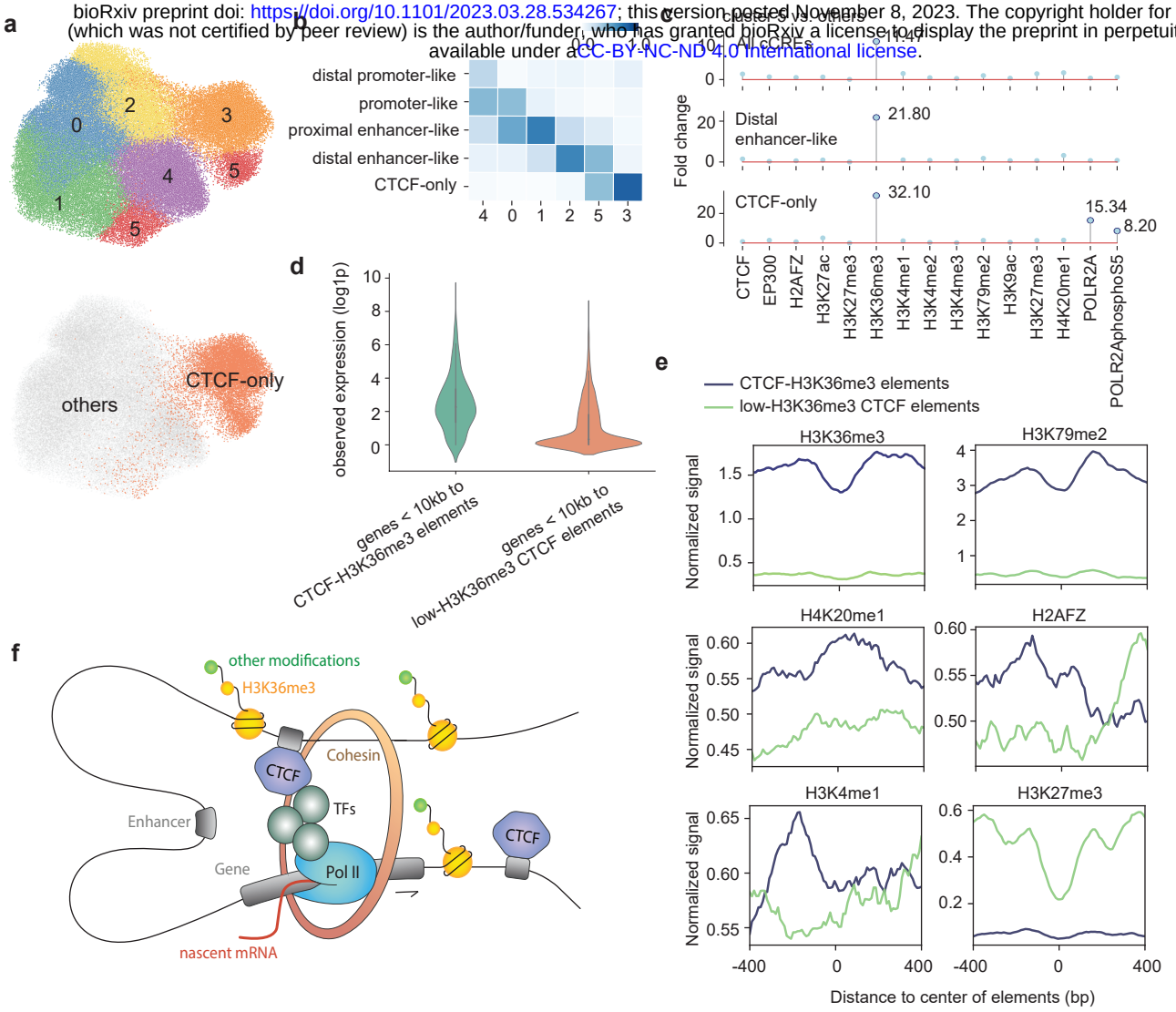

Figure 4. cCRE representations learned by CREaTor suggest a new role of CTCF-bound elements. a) Uniform Manifold Approximation and Projection (UMAP) of cCRE embeddings in K562. Upper: colored and numbered as clusters grouped by the Leiden algorithm. Bottom: colored and labeled by element type. **b)** Composition of different element types in each cluster by percentage. Proximal elements: elements falling within 200bp of an annotated TSS. Distal elements: elements more than 200bp from any annotated TSS. Promoter-like: elements with high DNase and H3K4me3 signals. Enhancer-like: elements with high DNase and H3K27ac signals. CTCF-only: elements with high DNase and CTCF signals, as well as low H3K4me3 and H3K27ac signals. **c)** Fold change of histone marker peaks of given types of cCREs in cluster 5 with respect to those in other clusters. Top: all cCREs. Middle: distal enhancer-like elements. Bottom: CTCF-only elements. **d)** Expression value (log1p) distribution of genes within 10kb of different types of CTCF-bound elements. **e)** Average signals of H3K36me3, H3K79me2, H4K20me1, H2AFZ, H3K4me1 and H3K27me3 on different types of CTCF-bound elements. **f)** Illustration for the proposed model of CTCF-H3K36me3 elements promoting transcription elongation.

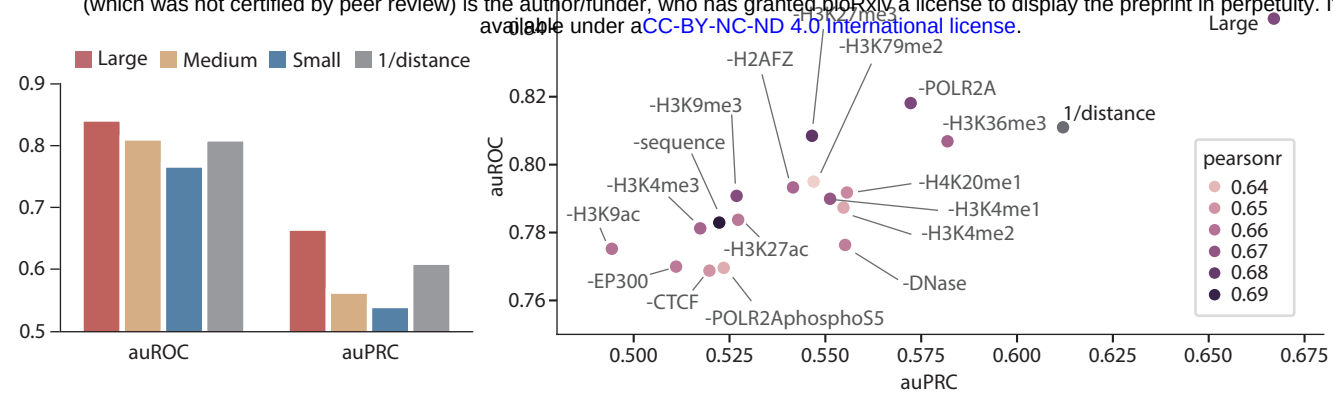

Figure 5. Feature ablation study demonstrates the importance of feature integration for modeling. a) auROC and auPRC of 4 different models on cCRE-gene pair classification. Large (red): the model trained with 17 types of features. Medium (yellow): the model trained with 8 types of features (genomic sequence, DNase, CTCF, H3K27ac, H3K4me3, H3K9ac, EP300, and POLR2AphosphoS5). Small (blue): the model trained with 5 types of features (genomic sequence, DNase, CTCF, H3K27ac, and H3K4me3). **b)** Large model trained with 17 types of features outperforms other models on cCRE-gene interaction classification tasks. Minus signs indicate the following type of feature is removed during model training. Labels (positive/negative) of cCRE-gene pairs were from the same source as Figure 2. The colors of dots indicate the Pearson r between observed and predicted expression of K562-specific genes.

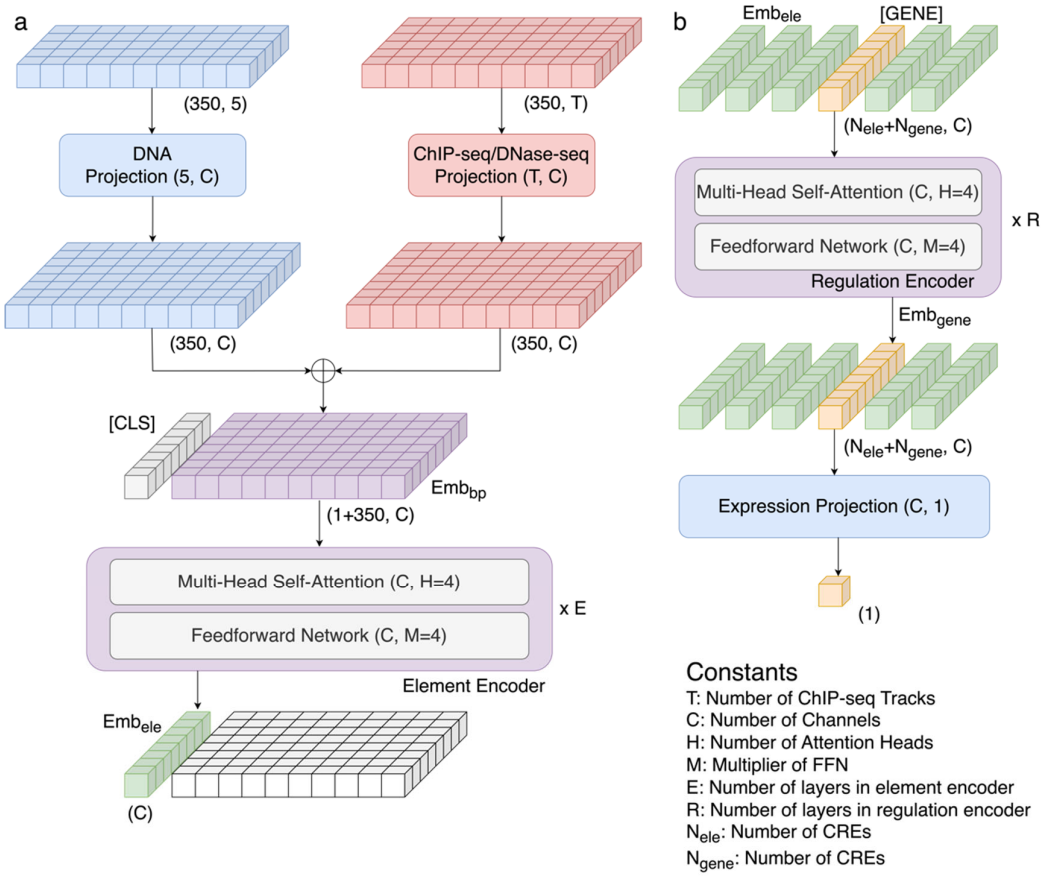

Extended Data Figure 1 | Architecture of CREaTor. CREaTor is composed of two modules. **a)** Element module encodes the representation of cCREs. We first map DNA and ChIP-seq/DNase-seq to latent space through a linear projection respectively, and then combine them through element-wise addition to obtain Emb_{bp}, the feature embedding of each bp. We feed the Emb_{bp}s into the element encoder together with a [CLS] token. The [CLS] token adaptively aggregates information from the Emb_{bp}s in the element encoder. We use the output vector of [CLS] token as the representation of the element, namely Emb_{ele}. **b)** Regulation module models the interaction between cCREs and genes. We concatenate the Emb_{ele} of cCREs (denoted in blue and yellow) and the [GENE] tokens (denoted in red) as the input of the regulation encoder. The [GENE] tokens interact with and are regulated by the cCREs in the regulation encoder. We apply a linear projection with SoftPlus activation on the output vector of [GENE] tokens to predict their expressions. The size of each component of the architecture is shown as a tuple inside the block. The shape of the tensor at each step is denoted as a tuple in the bottom right of the blocks.

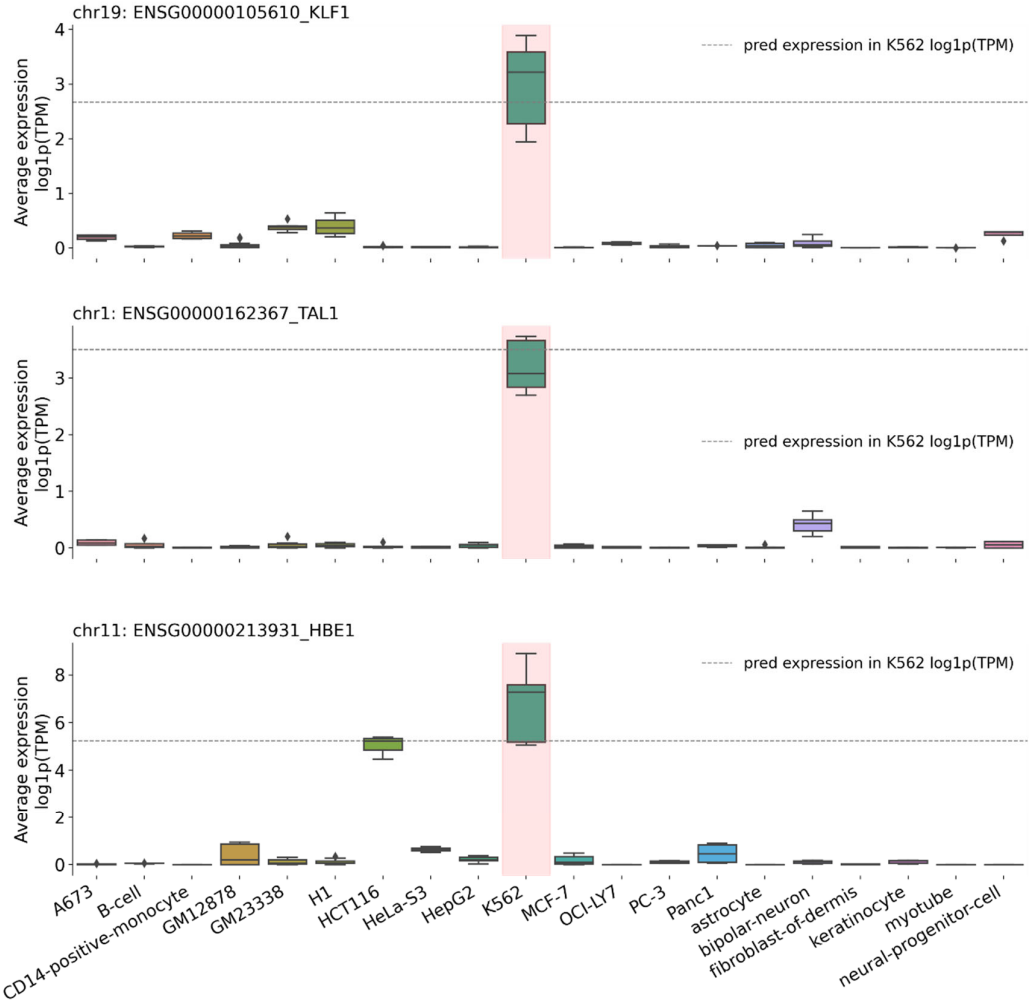

Extended Data Figure 2 | Prediction of K562 differentially expressed genes. Representative examples of observed and predicted expression of genes KLF1, TAL1 and HBE1 in 20 different types of cells. The dashed line indicates the predicted values.

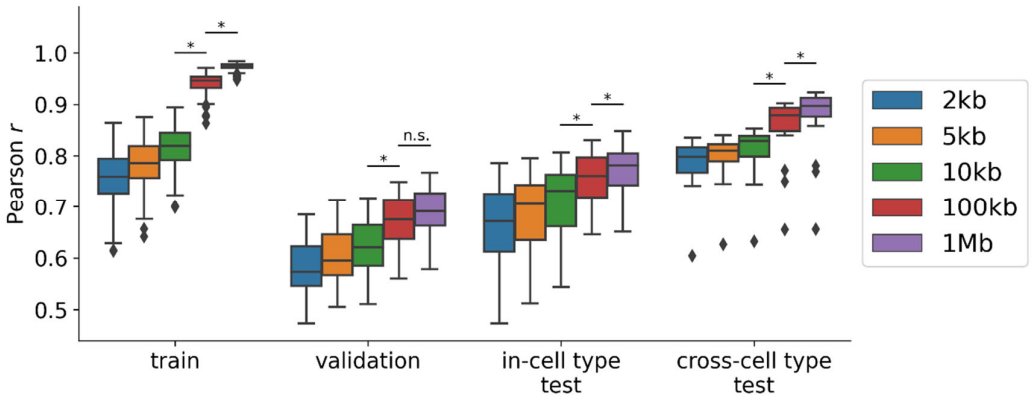

Extended Data Figure 3 | Performance of CREaTor with cCREs up to 2kb, 5kb, 10kb, 100kb, or 1Mb away from the TSS of target genes. The training set includes chr1-7, 10-15, and 17-22 in 19 cell types other than K562. The validation set includes chr16 in cell types other than K562. The in-cell type test set includes chr8 and chr9 in cell types other than K562. Cross-cell type test set represents all chromosomes in the K562 cell line. P values were computed with the two-sided Mann–Whitney U test.

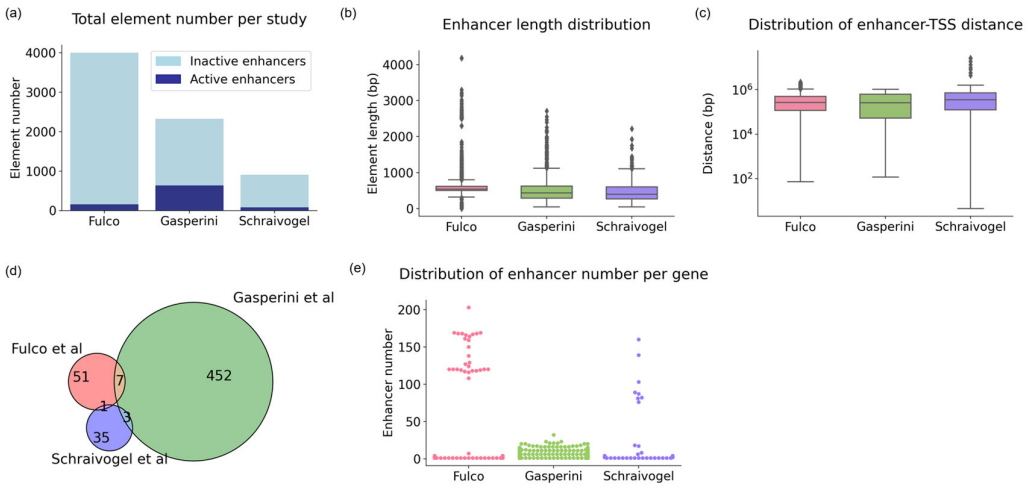

Extended Data Figure 4 | Statistics of enhancer-gene interaction data from 3 CRISPRi-based studies. The statistics were performed on data after genomic coordinates liftover and non-autosomosal data filtering. (a) The number of active and inactive enhancers tested by each study. (b) Enhancer length distribution in each study. (c) Enhancer-gene TSS distance distribution in each study. (d) Overlapped active enhancers in 3 studies. (e) The number of enhancers tested for each gene in each study.

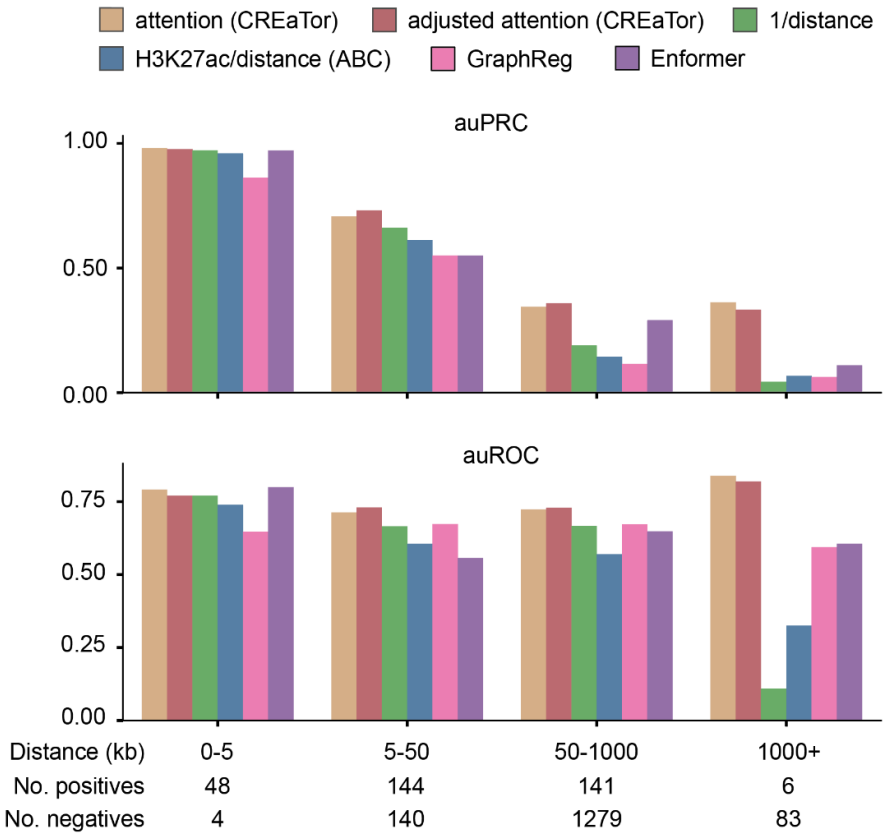

Extended Data Figure 5 | auPRC and auROC of CREaTor and its counterparts on the classification of cCRE-gene pairs collected from 3 independent CRISPR perturbation experiments. cCRE-gene pairs are stratified by their relative genomics distances. The number of positive/negative labels in each group is annotated at the bottom. Labels (positive/negative) of cCRE-gene pairs were collected from CRISPR perturbation experiments.

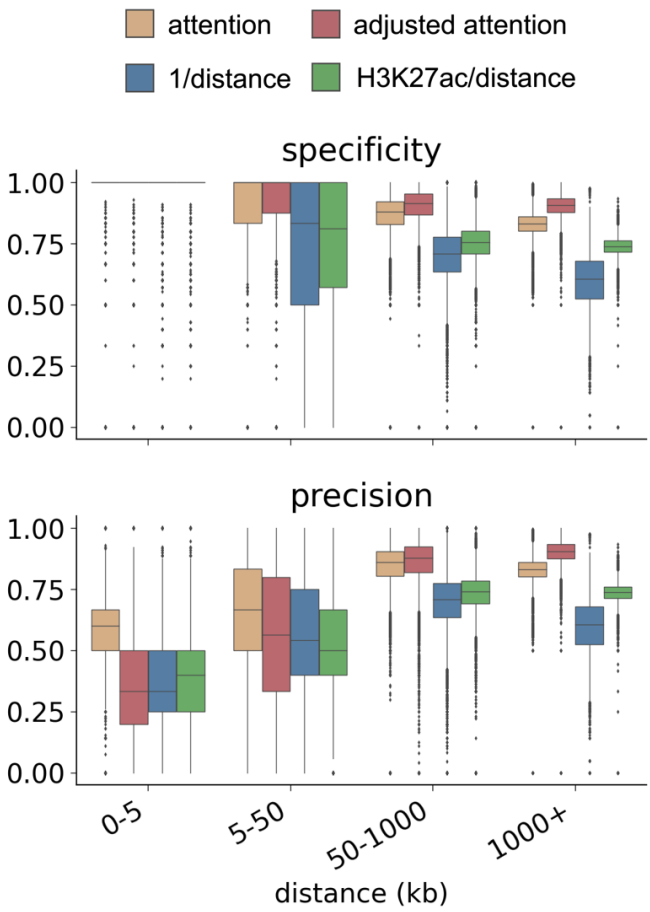

Extended Data Figure 6 | Specificity and precision scores of CREaTor and its counterparts on cCRE-gene pair classification. Distance denotes the relative genomic distance between cCREs and genes. The performance is evaluated for each gene and each distance group separately. The H3K27ac value of a cCRE is calculated as the sum of the H3K27ac peak values of the element. Positive/negative cutoff is set as mean values of attention scores in each distance group. Labels (positive/negative) of cCRE-gene pairs were collected from a Pol-II mediated ChIA-PET experiment of K562.

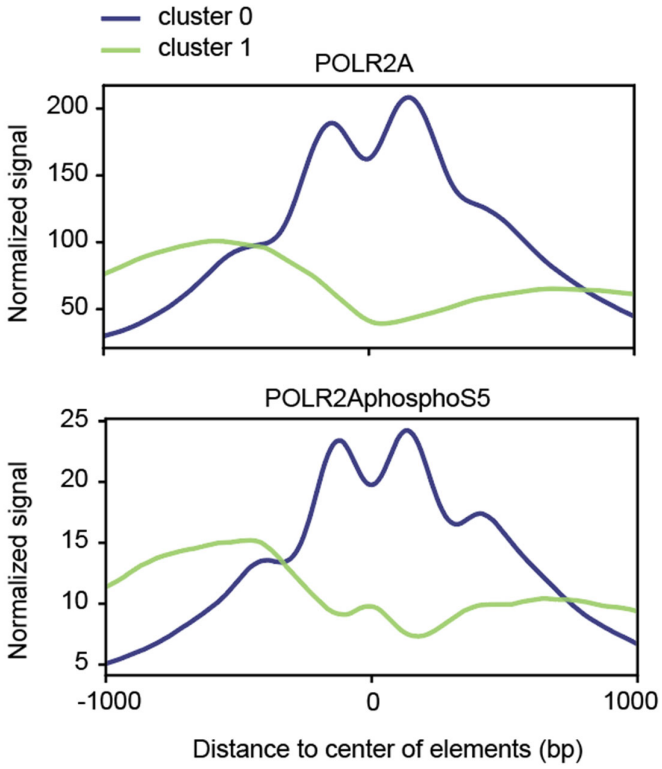

Extended Data Figure 7 | Average signals of RNA Pol II on cCREs in cluster 0 and cluster 1 respectively. Upper: unphosphorylated form of Pol II. Bottom: Pol II CTD phospho Ser5.

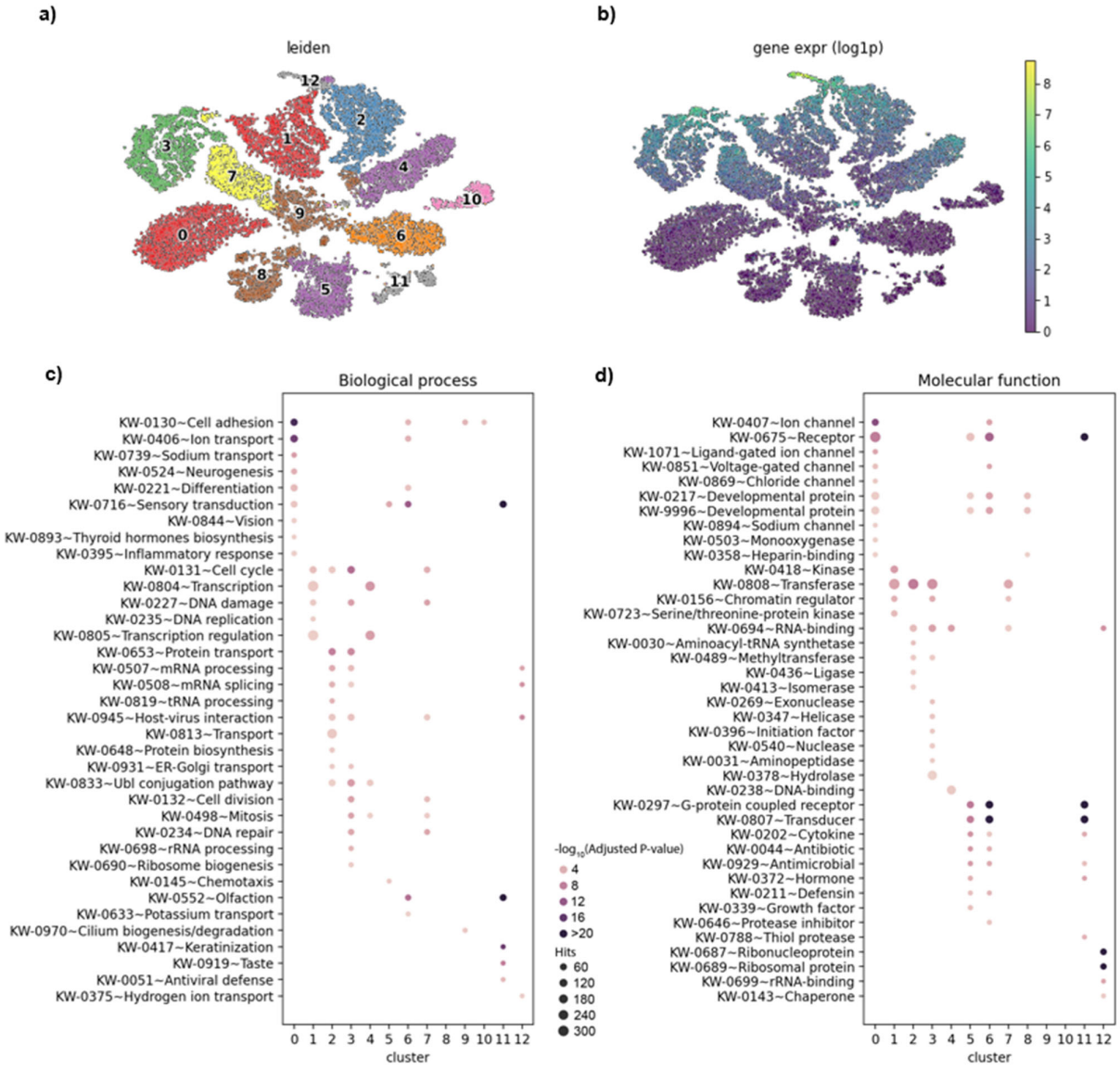

Extended Data Figure 8 | Gene representations learned by CREaTor can be clustered into groups with different functions. a) Uniform Manifold Approximation and Projection (UMAP) of gene embedding in K562, colored and numbered as clusters grouped by the Leiden algorithm. **b)** Same as (a), but colored by gene expression levels. **c)** Functional annotation clustering with the DAVID Gene Functional Classification Tool (DAVID, http://david.abcc.ncifcrf.gov) using UniProtKB biological process keywords. Significantly enriched (adjusted p-value<0.05) groups for genes in each cluster in (a) are shown. **d)** Functional annotation clustering with DAVID using UniProtKB molecular function keywords. Significantly enriched (adjusted p-value<0.05) groups for genes in each cluster in (a) are shown.